



Solar Cycle Variations in Meridional Flows and Rotational Shear within the Sun's Near-surface Shear Layer

Anisha Sen^{1,2} , S. P. Rajaguru¹ , Abhinav Govindan Iyer^{1,7} , Ruizhu Chen^{3,4} , Junwei Zhao⁴ , and Shukur Kholikov^{5,6}¹ Indian Institute of Astrophysics, II Block Koramangala, Bengaluru 560 034, India; anisha.sen@iiap.res.in, rajaguru@iiap.res.in² Pondicherry University, R. V. Nagar, Kalapet, Puducherry 605014, India³ Department of Physics, Stanford University, Stanford, CA 94305-4060, USA⁴ W. W. Hansen Experimental Physics Laboratory, Stanford University, Stanford, CA 94305-4085, USA⁵ National Solar Observatory, Boulder, CO, USA⁶ National Research University TIIAME, Kori Niyoziy 39, Tashkent 100000, Uzbekistan

Received 2024 October 11; revised 2025 March 28; accepted 2025 March 31; published 2025 April 22

Abstract

Using solar cycle–long helioseismic measurements of meridional and zonal flows in the near-surface shear layer (NSSL) of the Sun, we study their spatiotemporal variations and connections to active regions. We find that near-surface inflows toward active latitudes are part of a local circulation with an outflow away from them at depths around $0.97 R_{\odot}$, which is also the location where the deviations in the radial gradient of rotation change sign. These results, together with opposite signed changes, over latitude and depth, in the above quantities observed during the solar minimum period, point to the action of the Coriolis force on large-scale flows as the primary cause of changes in rotation gradient within the NSSL. We also find that such Coriolis force mediated changes in near-surface flows toward active latitudes only marginally change the amplitude of zonal flow and hence are not likely to be its driving force. Our measurements typically achieve a high signal-to-noise ratio ($>5\sigma$) for near-surface flows but can drop to 3σ near the base ($0.95 R_{\odot}$) of the NSSL. Close agreements between the depth profiles of changes in rotation gradient and in meridional flows measured from quite different global and local helioseismic techniques, respectively, show that the results are not dependent on the analysis techniques.

Unified Astronomy Thesaurus concepts: [The Sun \(1693\)](#); [Solar cycle \(1487\)](#); [Helioseismology \(709\)](#); [Solar activity \(1475\)](#); [Solar rotation \(1524\)](#); [Solar meridional circulation \(1874\)](#)

1. Introduction

The near-surface shear layer (NSSL; M. J. Thompson et al. 1996) of the Sun, situated just below the solar surface over depths to about 35 Mm, is marked by a swift increase in the rotation rate as depth increases (J. Schou et al. 1998). Several helioseismic studies (T. Corbard & M. J. Thompson 2002; H. M. Antia & S. Basu 2010; A. Berekat et al. 2014, 2016; H. M. Antia & S. Basu 2022) have since established its overall structure, and the later ones have also uncovered changes, over space and time, that relate to active region magnetic fields and the solar cycle. These latter solar cycle–related changes connect the NSSL to the already well-studied zonal flows or torsional oscillations that extend almost throughout the convection zone (H. M. Antia & S. Basu 2001; S. V. Vorontsov et al. 2002). The structure and dynamics of the NSSL uncovered by helioseismology so far (A. Berekat et al. 2016; H. M. Antia & S. Basu 2022) pose challenges to theoretical and simulation studies (M. S. Miesch 2000; L. L. Kitchatinov 2016; L. I. Matilsky et al. 2019; L. L. Kitchatinov 2023) and have also served to emphasize it as an important region where complex magnetohydrodynamic processes controlling the magnetic activity of the Sun play out. These latter aspects have attracted the attention of modelers in exploring the role of NSSL in dynamo processes (M. Dikpati et al. 2002;

A. Brandenburg 2005; V. V. Pipin & A. G. Kosovichev 2011; B. B. Karak & R. Cameron 2016).

Although the zonal and meridional flows extend throughout the convection zone straddling the NSSL, probing solar cycle–related changes in them within it is expected to give clues to understanding the origin not only of these flows but also of the NSSL and its maintenance (L. L. Kitchatinov 2016; L. I. Matilsky et al. 2019). In this connection, understanding the dynamics of large-scale inflows toward active regions (L. Gizon et al. 2001; D. A. Haber et al. 2004; B. W. Hindman et al. 2009; D. C. Braun 2019) and their cumulative contributions to the changes in zonal (H. M. Antia & S. Basu 2022) and meridional flows (P. L. Poulter et al. 2022; S. S. Mahajan et al. 2023) is important. Given that the Coriolis force plays a central role in the redistribution of angular momentum over depth (A. Lebedinsky 1941; L. L. Kitchatinov 2016), it will be interesting to examine how such forces on flows around active regions contribute to the changes in the NSSL. In fact, H. C. Spruit (2003) presented a model for the zonal flows in terms of geostrophic flows driven by subsurface temperature variations caused by the increased radiative losses through the plages and small-scale magnetic fields surrounding sunspots. Helioseismic measurements, using the ring diagram technique, showed that sunspots and surrounding plages drive a mean inflow with speeds of $20\text{--}30\text{ m s}^{-1}$ and cyclonic circulation of 5 m s^{-1} around their edges (B. W. Hindman et al. 2009). The overall contributions of such flows to the variations in meridional flows have been assessed by P. L. Poulter et al. (2022) and S. S. Mahajan et al. (2023). These authors have concluded that there remain significant solar cycle variations in the meridional flows near the surface, even after removing active region inflows. For solar cycle 24 and the early part of cycle 25,

⁷ Currently at Sydney Institute for Astronomy, School of Physics, The University of Sydney, NSW 2006, Australia.



S. S. Mahajan et al. (2023) deduced that the variations in the background meridional flow are largely due to active regions, whereas the torsional oscillation remains a universal phenomenon, as its magnitude or phase shows no significant alteration when active region neighborhoods are excluded. H. M. Antia & S. Basu (2022) have shown that the radial gradient of the solar rotation rate is influenced by the solar cycle, exhibiting more significant changes in active latitudes than in neighboring higher latitudes.

In this Letter, through a joint analysis of helioseismic measurements of meridional and zonal flows, we explore the depth structure of changes due to flows around active regions and examine how they influence the gradient of solar rotation and its variation over depth and time within the NSSL. The rest of the Letter is structured as follows: Section 2 outlines the data utilized, followed by a description of the analysis technique in Section 3. Section 4 presents our findings, and Section 5 discusses the implications of our results.

2. Data

We use helioseismic data from the spaceborne Helioseismic and Magnetic Imager (HMI; P. H. Scherrer et al. 2012) on board NASA’s Solar Dynamics Observatory (SDO), which has been observing the Sun since 2010 March. For seismic inversions of solar interior rotation rate and changes (zonal flows) in it, we have used oscillation frequencies and their splittings measured from the HMI 72-day time series of spherical harmonic coefficients of global oscillation modes (series `hmi.V_sht_modes`; H. M. Antia & S. Basu 2022). The 72 day data sets we have used start from set number 6328 with date 2010 April 30 and end at set number 10720 with date 2022 July 22.

For time–distance (TD) helioseismic measurements of meridional flow, we use the HMI/SDO Dopplergrams with a 45 s cadence, spanning 13 yr from 2010 May to 2023 April. Each day’s data are tracked and Postel remapped to account for solar rotation and projection effects using the Stanford Joint Science Operations Center (JSOC) helioseismology pipeline, following the procedures described by J. Zhao et al. (2013). Additionally, we utilize identically processed Global Oscillation Network Group (GONG) data for the same meridional flow measurements. The network-merged data, obtained from GONG stations around the globe over the same time period, are used in this study. The final data products used for travel-time measurements, from both HMI and GONG, have a binned down spatial resolution of $0.36 \text{ deg pix}^{-1}$.

We also employ local TD helioseismic inversions for horizontal velocity fields (J. Zhao et al. 2012a), publicly available in the JSOC TD helioseismology pipeline,⁸ along with the HMI line-of-sight (LOS) magnetograms, to check and establish connections between flows around individual active regions and our measurements of global-scale changes in meridional and zonal flows. For comparing time–latitude profiles of flows with those of sunspots, we use data on the latter from the National Oceanic and Atmospheric Administration’s Solar Region Summary.

3. Analysis Techniques

3.1. Meridional Flow

We measure travel times of acoustic waves (p modes) that propagate between two surface locations, connected by a path through the interior, using the technique of TD helioseismology (T. L. Duvall et al. 1993). The measurement geometry involves

north–south (N–S) and west–east (W–E) oriented arcs (36° wide) for measuring the meridional flows and the center-to-limb systematics (CLSs; J. Zhao et al. 2012b), respectively, employing the “point-to-point” cross correlation of the Doppler signals as explained in S. P. Rajaguru & H. M. Antia (2015). The CLSs in travel times are removed following the same procedure as originally suggested by J. Zhao et al. (2012b) and adopted in almost all TD measurements of meridional circulation to date. Both the HMI and GONG data sets are processed and subjected to exactly the same method of analysis, and the measurements used here are part of an ongoing detailed study (R. Chen et al. 2025, in preparation) to understand the additional systematic differences between GONG and HMI travel times reported by L. Gizon et al. (2020). These additional systematics affect inferences only of deeper (below $0.9 R_\odot$) layers and also change slowly over solar cycle timescales. Since we are studying changes in meridional flows by subtracting a long time average (over the solar cycle) from each 1 yr running average solution obtained at each month, much of the systematics gets subtracted out too. Additionally, to take care of the surface magnetic effect in flow measurements (Z.-C. Liang & D.-Y. Chou 2015; R. Chen & J. Zhao 2017), we mask out active regions in input Doppler data that exceed a threshold of 40 G in the $0.36 \text{ deg pix}^{-1}$ resolution HMI LOS magnetograms. Note that we recover meridional flows from the inversions for the stream function, which satisfies the continuity equation, and thus the mass conservation constraint is built into the inversion scheme (S. P. Rajaguru & H. M. Antia 2015).

3.2. Zonal Flow

Solar interior rotation rate as a function of radius (r), latitude (θ), and time (t), $\Omega = \Omega(r, \theta, t)$, is determined through seismic inversions of oscillation frequency splittings (described in Section 2) by adapting the 2D regularized least-squares technique (H. M. Antia et al. 1998). The rotation rate is represented as a product of cubic B-splines in solar radius and cosine of the colatitude. Twenty uniformly spaced knots or nodes in the cosine of colatitude, and 50 knots in the acoustic radius, have been used for inversion. Since the main goal is to study changes in the NSSL, we calculate residuals by subtracting solar cycle–long averages. Our data sets covered cycle 24 and the initial part of cycle 25; however, we subtract only the cycle 24 average from the individual measurements. Thus the residual rotation rate is given by $\delta\Omega(r, \theta, t) = \Omega - \langle \Omega \rangle_{C24}(r, \theta)$, and the residual of the dimensionless radial gradient of rotation rate (H. M. Antia & S. Basu 2022; residual rotational shear hereafter)⁹ is $\delta(\partial \log \Omega / \partial \log r)(r, \theta, t) = (\partial \log \Omega / \partial \log r) - \langle \partial \log \Omega / \partial \log r \rangle_{C24}$, where $\langle \rangle_{C24}$ stands for time average over cycle 24. We apply a 1 yr running mean to smooth out the fluctuations in the measurements at each r and θ .

4. Results

4.1. Relations between Residual Rotational Shear and Meridional Flow

Variations over time and latitude in the residual rotational shear, $\delta(\partial \log \Omega / \partial \log r)$, and in residual meridional flows, δU_θ , are shown in Figure 1 for the surface layers ($0.99 R_\odot$, left

⁹ Rotation inversions used here are the same as published by H. M. Antia & S. Basu (2022), with the addition of about 1 yr longer data sets, and were provided by H. M. Antia.

⁸ <http://jsoc.stanford.edu/data/timed/>

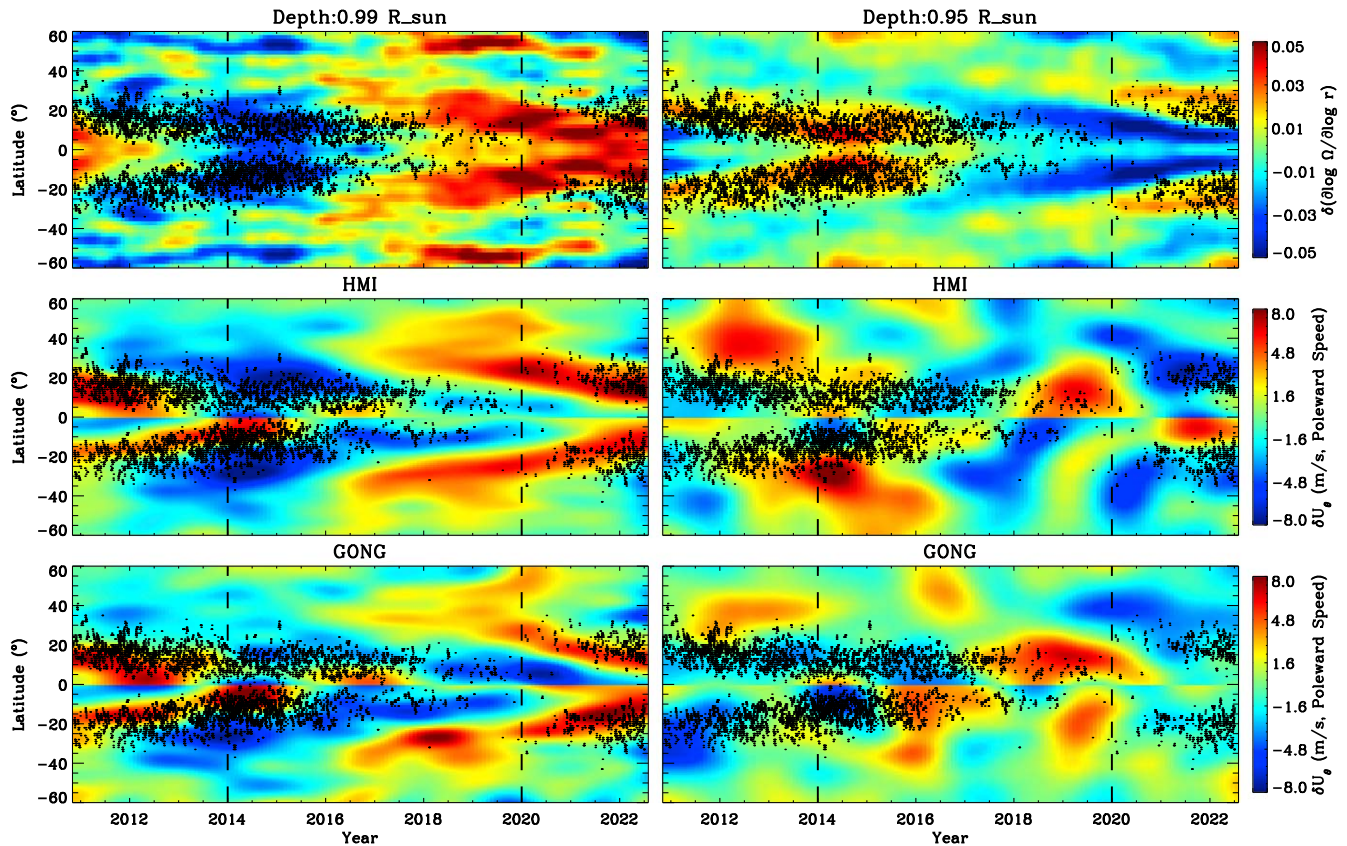


Figure 1. Changes (cycle 24 subtracted) in dimensionless radial gradient of rotation rate, $\delta(\partial \log \Omega / \partial \log r)$, from HMI global helioseismic rotation inversions (top panels) and those in the meridional flow, δU_{θ} (middle and bottom panels from HMI and GONG, respectively) as a function of latitude and time at $0.99 R_{\odot}$ (left) and at $0.95 R_{\odot}$ (right). Sunspot locations are overlotted as black dots. The two vertical dashed lines mark the cycle 24 maximum (2014) and minimum (2020).

panels) and for the bottom layers ($0.95 R_{\odot}$, right panels) of the NSSL. The striking depth and latitudinal dependence of changes in rotation gradient within the NSSL have already been presented (A. Berek et al. 2016; H. M. Antia & S. Basu 2022; except that results here cover longer into cycle 25): near $0.95 R_{\odot}$, sunspot latitudes coincide with the radial gradient of rotation being less (in magnitude) than average (over the solar cycle), while those in the near-surface layers (above the depth of $0.98 R_{\odot}$) coincide with it being larger than average. Note that radial gradient itself is negative in the NSSL, and hence a negative value for changes in it means it is steeper than average and vice versa. The opposite signs of changes at active latitudes at depths $0.99 R_{\odot}$ and $0.95 R_{\odot}$ are clear. The sign change happens around the depth of $0.97 R_{\odot}$, and we focus on it later in this section. Note that the global helioseismic measurements are hemisphere symmetric, i.e., they are insensitive to hemisphere asymmetric changes.

The time–latitude profiles of δU_{θ} measured using HMI and GONG data are shown in the middle and bottom panels of Figure 1. Note that, in our sign convention, positive values (red) correspond to poleward and negative (blue) to equatorward flows, and hence any cross-equator flow exhibits a discontinuity in colors across the equator in these panels. As already well established (B. W. Hindman et al. 2009; D. C. Braun 2019; P. L. Poulter et al. 2022; S. S. Mahajan et al. 2023), active regions drive an inflow toward themselves from the neighboring quiet-Sun areas in the near-surface layers. Such flows manifest as negative changes on the poleward side and as positive changes on the equatorward side of the active belt in the panels for δU_{θ} at $0.99 R_{\odot}$ in Figure 1; the

$\delta(\partial \log \Omega / \partial \log r)$ follow suit with a correlated variation. During the solar minimum period, enhanced poleward meridional flow ($\delta U_{\theta} > 0$) coincides with a less than average residual rotational shear ($\delta(\partial \log \Omega / \partial \log r) > 0$). These results clearly implicate the W–E (rotational) component of the Coriolis force, $-2\Omega \times \delta U$.

Below $0.97 R_{\odot}$, the δU_{θ} reverses sign ($0.95 R_{\odot}$ panels in Figure 1). Active latitudes are flanked by outflows on either side indicating circulation cells that connect to surface inflows. Note that these outflow signals are patchy, and we discuss them further below. During the cycle minimum period, a negative δU_{θ} appears indicating a return flow from about 50° latitude toward the equator, possibly fed by the enhanced near-surface poleward flow. Although a correlated negative $\delta(\partial \log \Omega / \partial \log r)$ appears at low latitudes, its latitudinal extent, unlike in the near-surface layers, is narrow and lacks a clear correspondence with δU_{θ} . We discuss possible physical causes for this again in Section 5. Moreover, the latitude extent of the cycle minimum circulation cell gradually decreases from the higher latitude side and becomes the equator-side circulation of the migrating zonal (activity) band of the next cycle.

We point out that the patchiness of δU_{θ} at $0.95 R_{\odot}$ is likely related to the situation of only large active regions driving significant outflows at depths beneath 10–15 Mm (D. A. Haber et al. 2004) and also that such signals are significantly above noise levels. For example, in the HMI results for solar maximum (see Figure 2), the outflow signals on the poleward side of active latitudes (between 20° and 40°) are in the range of $3\text{--}8 \text{ m s}^{-1}$, with estimated errors ranging from 0.3 to 1.1 m s^{-1} , and hence signal levels are 3σ or higher. Here, errors

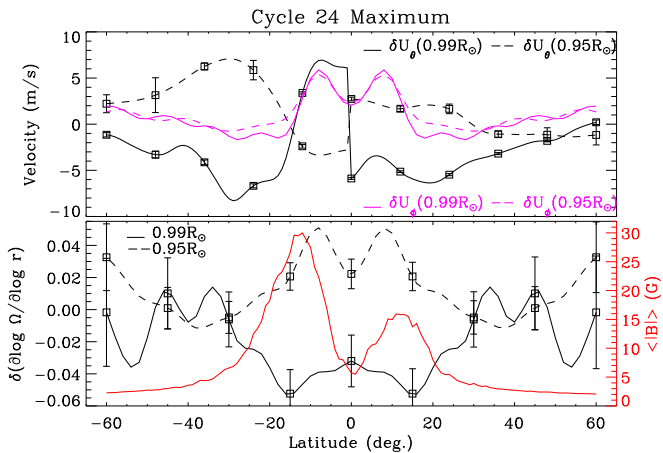


Figure 2. Latitude profiles of changes in meridional flow (δU_θ , in black) and zonal flow (δU_ϕ , in pink), averaged over 1 yr around the cycle 24 maximum, for depths $0.99 R_\odot$ (solid) and $0.95 R_\odot$ (dashed) in the top panel. The same in the radial gradient of rotation, $\delta(\partial \log \Omega / \partial \log r)$, along with the longitudinally averaged unsigned magnetic field (right y-axis), is shown in the lower panel. The error bars shown represent errors estimated in the inversion method (see Section 4.1 for details).

are calculated from inverted flow velocities determined by repeating the inversions 1000 times with travel times randomly perturbed with estimated errors in observed values (S. P. Rajaguru & H. M. Antia 2015). Further, a significant part of the patchiness near the equator is due to cross-equator flows (R. Komm 2022; S. S. Mahajan et al. 2023), and we defer a detailed analysis of them to a separate study. We note that a 3 yr smoothing brings out the correlated variations in δU_θ and $\delta(\partial \log \Omega / \partial \log r)$ at $0.95 R_\odot$ much more clearly (not shown). GONG and HMI results for δU_θ agree well overall for the dominant features discussed above, increasing their reliability. However, GONG observations lack sensitivity to flows very near the surface (L. Gizon et al. 2020; H. M. Antia & S. Basu 2022) and consequently suffer noisy fluctuations throughout the near-surface layers, especially at higher latitudes. For all of our further presentation in this Letter, we use only HMI results.

To understand better the spatial associations between active latitudes and the flows, we plot latitude profiles of the latter averaged over 1 yr (2014–2015) around the solar maximum in Figure 2: residual meridional flows (δU_θ , in black) and zonal flows (δU_ϕ , in pink) are shown in the upper panel, and $\delta(\partial \log \Omega / \partial \log r)$ along with the longitudinally averaged unsigned magnetic field (calculated from HMI LOS magnetograms) in the lower panel; solid and dashed curves are for depth $0.99 R_\odot$ and $0.95 R_\odot$, respectively. We note a few important features in the spatial association between the above quantities. (i) In the near-surface ($0.99 R_\odot$) layers, the latitudinal extent and signs of $\delta(\partial \log \Omega / \partial \log r)$ match with those of δU_θ , as expected of the action of the Coriolis force on the latter; near the base of the NSSL ($0.95 R_\odot$, black dashed curves), however, the former’s latitudinal structure coincides with the zonal flow (δU_ϕ) itself, while its sign correlates with that of the poleward side δU_θ . Note that the cross-equator flows driven by N–S asymmetry in active regions appear as discontinuities at the equator in Figure 2 due to our sign convention. (ii) The zonal flows (δU_ϕ) peak on the equatorward side of active belt (H. C. Spruit 2003), with a slight enhancement on the poleward side (at $0.95 R_\odot$) because of

the outflow ($\delta U_\theta > 0$) on that side. (iii) A clear association between the N–S asymmetry in the magnetic field and that in δU_θ (upper panel of Figure 2) for both the inflows and outflows is evident; more interestingly, outflows at $0.95 R_\odot$ (dashed curve) show a larger N–S asymmetry in proportion to that in the magnetic field than the inflows near the surface do. Features (i) and (ii) above together show that the horizontal parts of flows toward active latitudes (δU_θ) and the action of the Coriolis force on them only minimally alter the zonal flow amplitudes and hence cannot be their cause.

Correlated change of sign over time and depth of residual meridional flows and rotation gradient within the NSSL is the most striking feature of our results in Figure 1. To bring out clearly such connections between δU_θ and $\delta(\partial \log \Omega / \partial \log r)$, we plot their time–depth profiles in Figure 3. In view of the latitudinal associations brought out above (Figure 2), it is useful to relate the depth profiles of δU_θ over latitudes slightly higher than those of the rotation gradients, and hence we choose latitudes 20° , 25° , and 30° for the former (top and middle rows of Figure 3 for the north and the south, respectively) and 10° , 15° , and 20° (bottom row of Figure 3) for the latter. During cycle maximum, the prominent equatorward flows (blue) seen from the surface down to depths of $\approx 0.97 R_\odot$, in both hemispheres, are the inflows toward the active latitudes. At depths below $0.97 R_\odot$, these inflows change direction toward the poles (red), indicating a local circulation connected by downflows beneath active latitudes. Near the active latitudes (20° and 25°), the strength of this return flow (poleward) away from active latitudes, over depths 0.94 – $0.97 R_\odot$, is stronger in the southern hemisphere than in the north, clearly correlating with the amount of magnetic flux (or the hemispheric asymmetry in the active region magnetic fields). We note that this hemispheric difference in peak flows at $0.95 R_\odot$ (dashed curve in the upper panel of Figure 2) during solar maximum is about 5 m s^{-1} while the noise levels are in the range of 0.3 to 1.1 m s^{-1} . During cycle minimum, the residual flows have the opposite structure over depth. The above time–depth profiles of δU_θ clearly show a strong correlation with $\delta(\partial \log \Omega / \partial \log r)$, shown in the bottom row of Figure 3. We point out that, as can be discerned by a close comparison of depth profiles, the change from inflows to outflows in δU_θ happens at a slightly shallower depth than for that in $\delta(\partial \log \Omega / \partial \log r)$. Such a difference is entirely in order if the Coriolis force acting on the former is the cause of the changes in the latter, which should occur at the sign change of the depth gradient of the flow rather than that of the flow itself. It is also interesting to note that the hemispheric change in δU_θ over time occurred earlier in the north, in correlation with hemispheric activity maxima.

4.2. Flows around an Active Region

Among a good number of studies of flows around active regions (e.g., D. A. Haber et al. 2004; B. W. Hindman et al. 2009; D. C. Braun 2019; N. Gottschling et al. 2021; P. L. Poulter et al. 2022; S. S. Mahajan et al. 2023), the former two that employed ring diagram analysis have shown the existence of outflows at deeper layers beneath large active regions. Here, to ascertain further that the changes we measure in meridional flows in fact relate to the flows around active regions, especially to depths down to $0.97 R_\odot$, we examine 3D (latitude, longitude, depth) local TD helioseismic inversions for horizontal velocity fields available in the JSOC TD

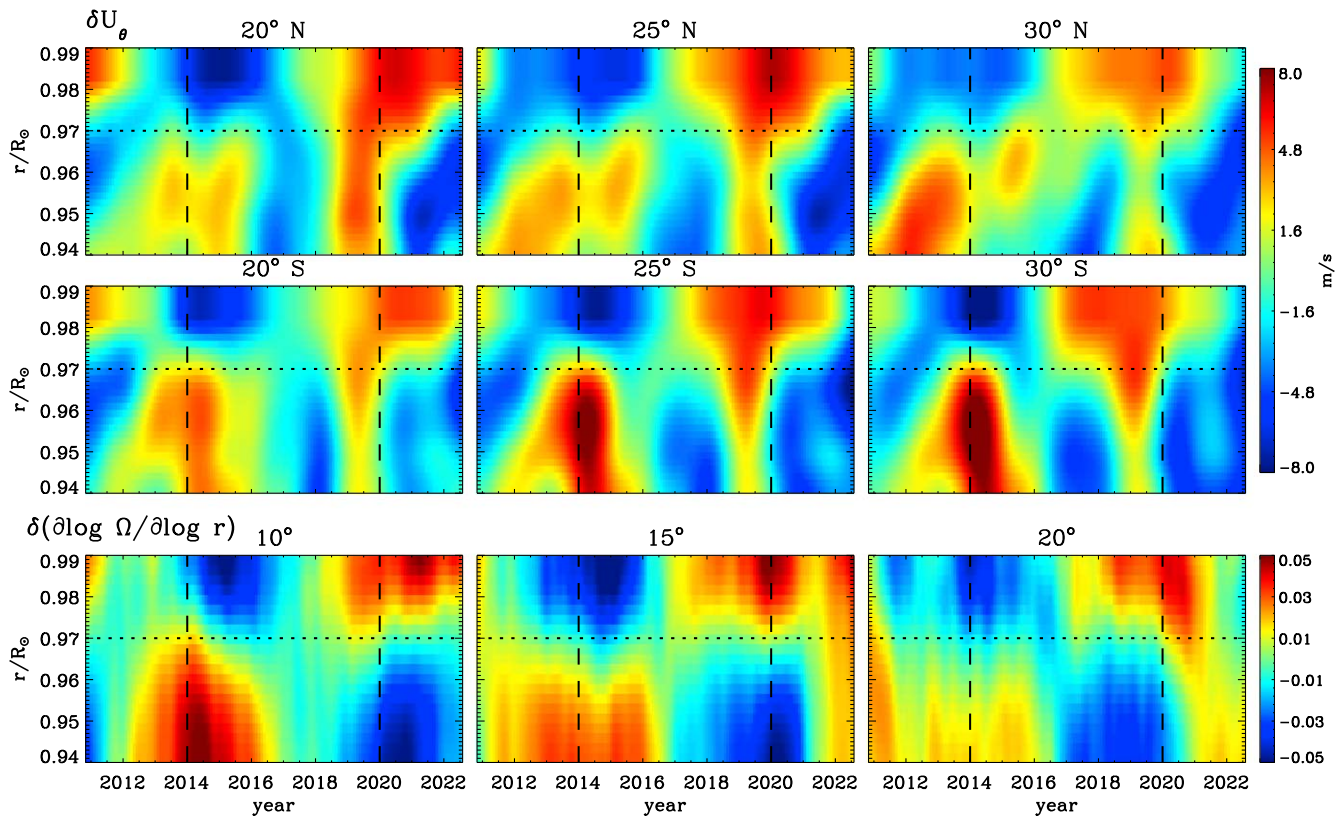


Figure 3. Connections between the time vs. depth profiles of changes in meridional flow (δU_θ) and those in the radial gradient of rotation ($\delta(\partial \log \Omega / \partial \log r)$). The top and middle panels show δU_θ for the northern and southern latitudes (20° , 25° , and 30°), respectively. The north–south symmetric component of changes in $\delta(\partial \log \Omega / \partial \log r)$ is shown in the bottom row for latitudes 10° , 15° , and 20° . The two vertical dashed lines in each panel mark the cycle 24 maximum (2014) and minimum (2020), and the horizontal dotted lines mark the depth $0.97 R_\odot$. All the results here are from the HMI data.

helioseismology pipeline (J. Zhao et al. 2012a). We remove the CLSs in these full-disk flow maps, stacked from $30^\circ \times 30^\circ$ tiles, and the large-scale time-averaged background flows (rotation and meridional flows) following S. S. Mahajan et al. (2023). We note that these TD pipeline measurements do not mask out the strong magnetic field umbral pixels and hence are subject to artifacts in flow inferences over the spot area including the moat flow ($\sim 50 \text{ m s}^{-1}$) that extend 10–20 Mm beyond the penumbra (B. W. Hindman et al. 2009); however, we are concerned with flows surrounding the spots on a larger scale ($\sim 100 \text{ Mm}$), where such artifacts are negligible, and moreover we smooth the flow maps on scales of 20 Mm. An example map of flows around a large active region, NOAA 12192 (S12W08), observed on 2014 October 23 is shown in Figure 4. The flows, plotted as arrows here, are averaged over the near-surface depths of 0–3 Mm (left panel) and over 13–21 Mm (right panel). It is clear that there is a large-scale inflow, starting from around a distance of 100–150 Mm away from the spot region, drawing fluid from the quiet Sun. These converging flows near the surface sink down closer to the spots and drive an outflow at depths below about 13 Mm (right panel of Figure 4).

On average, the Coriolis force causes cyclonic inflows (B. W. Hindman et al. 2009; D. C. Braun 2019) and anticyclonic outflows: a sketch of the average flow patterns in the northern hemisphere, along with their influence on the rotation gradient, is shown in Figure 5; note that the active region shown in Figure 4 belongs to the southern hemisphere and hence a flow structure opposite to that shown in Figure 5

will apply. We note that flows around an individual active region will always have deviations over smaller scales and due to complexities in magnetic structure; an averaging over several active regions is typically needed to bring out the Coriolis force influence on the flows. The average structure in Figure 5 is consistent with our main inferences on changes in meridional and zonal flow gradients (Figures 1, 2, and 3), which result from the collective (longitudinally averaged) contributions of all active regions over each measurement period. We however note that further detailed analyses are needed in light of the most recent findings of D. C. Braun (2024; see Section 5).

We point out that the transition to outflows for individual active regions happens at depths shallower than $0.97 R_\odot$, slightly different from the inferences in our global measurements (Figures 1, 2, and 3). This could result from the averaging involved in meridional flow measurements, and could be examined in detail in future studies.

5. Discussion and Conclusion

In this work, through a joint analysis of the radial gradient of rotation and meridional flows from global and local helioseismic measurements, respectively, we have studied in detail the solar cycle-related changes in these within the NSSL. We find that (Figures 1 and 2), between 0.97 and $0.99 R_\odot$, the steeper than average radial gradient of rotation ($\delta(\partial \log \Omega / \partial \log r) < 0$) on the poleward side of active region latitudes is due to inflows ($\delta U_\theta < 0$) directed toward them from higher latitudes. At depths below $0.97 R_\odot$, the smaller than average radial gradient of rotation ($\delta(\partial \log \Omega / \partial \log r) > 0$) is observed to accompany outflows

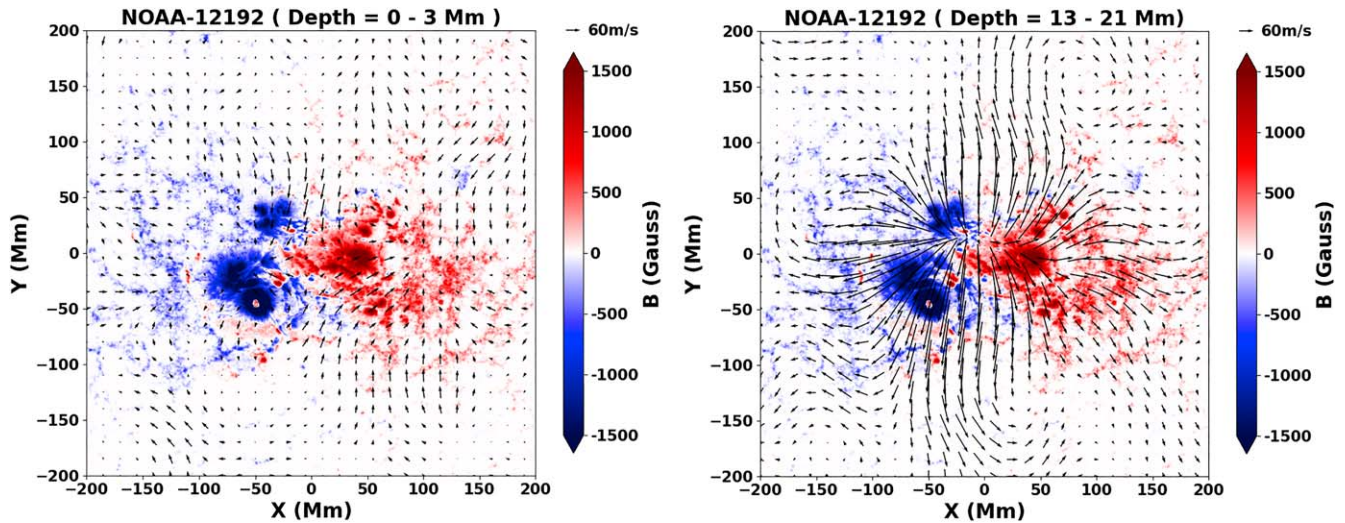


Figure 4. Local time–distance helioseismic inversions for flows around a large active region, NOAA 12192 (S12W08), observed on 2014 October 23. The flows, plotted as arrows here, are averaged over the near-surface depths of 0–3 Mm ($\approx 0.99 R_{\odot}$, left panel) and over 13–21 Mm ($\approx 0.97 R_{\odot}$, right panel). The background color image is the LOS magnetic field map of the bipolar spot region.

($\delta U_{\theta} > 0$) away from active latitudes, indicating a local circulation connected by downflows beneath them. A similar circulation cell on the equatorward side of active regions has a sign-reversed structure of above residuals in flows and rotation gradient.

The above connections between residual meridional flows and rotational shear arise from the action of the Coriolis force on active region flows, whose average structure in the northern hemisphere is depicted in Figure 5. Longitudinal averaging of flows around large numbers of active regions cancels out the inflows in the W–E (rotational) direction (S. S. Mahajan et al. 2023), and the resulting residual meridional flows take the form of circulation cells on either side of active latitudes as described above. In the context here, the relevant term in the W–E (or azimuthal) component of the Coriolis force is the one involving the meridional component of flow: $-2(\mathbf{\Omega} \times \delta \mathbf{U})_{\phi} = 2\Omega \sin(\theta) \delta U_{\theta}$, which for equatorward flow ($\delta U_{\theta} < 0$) is eastward (negative ϕ direction) on the Sun and the reverse for poleward flow ($\delta U_{\theta} > 0$), i.e., the inflows form a cyclonic circulation because of the Coriolis force. Such flows thus tend to slow down the zonal flows on their poleward side, resulting in the steeper radial gradient near the surface and the opposite result at depths below $0.97 R_{\odot}$, where the inflows turn into outflows away from active latitudes. Similarly, on the equatorward side of the active belt, the opposite influence of flows causes weaker radial gradient (in magnitude) near the surface and vice versa for deeper layers, but with a reduced effect at low latitudes because of the $\sin(\theta)$ term. Here, if the inflows toward an active region develop responding to a horizontal pressure gradient set up by whatever process, say for example by thermal causes, then its balancing with the Coriolis force will tend to drive the flows geostrophic at low Rossby numbers (H. C. Spruit 2003). During solar minima, near-surface equatorward flows ($\delta U_{\theta} < 0$) at active latitudes are replaced with enhanced poleward flows (Figures 1 and 3), which appear to drive a return flow around $0.95 R_{\odot}$ from about 50° latitude toward the equator. Although such solar minimum flows raise the question of their origin, the action of the Coriolis force on them is consistent with the sign change over depth in $\delta(\partial \log \Omega / \partial \log r)$.

An important aspect of active region flows has been their cumulative contributions to global-scale flows and influence on

magnetic flux transport (R. H. Cameron & M. Schüssler 2012; K. Teweldebirhan et al. 2024). We note that several studies have examined the level of contribution from active regions to global-scale changes in meridional flows, with differing conclusions (I. González Hernández et al. 2008; R. H. Cameron & M. Schüssler 2010; P. L. Poulter et al. 2022; S. S. Mahajan et al. 2023). Our main finding, viz., that the Coriolis force mediation of active region flows is the primary cause of correlated variations of δU_{θ} and $\delta(\partial \log \Omega / \partial \log r)$ (Figures 1–3), largely aligns with the case of δU_{θ} representing the longitudinally averaged collective contributions of active region flows (H. C. Spruit 2003; R. H. Cameron & M. Schüssler 2010; D. C. Braun 2019). The most recent detailed analyses of D. C. Braun (2024), however, show that active region flows alone cannot explain the δU_{θ} . Extending our analyses of connections between δU_{θ} and $\delta(\partial \log \Omega / \partial \log r)$ to the level of individual active regions over depths down to the base of the NSSL would be an additional avenue to probe the above issues. Hence, we plan on improving the TD helioseismic pipeline measurements (J. Zhao et al. 2012a) with larger patches (than the present $30^{\circ} \times 30^{\circ}$ tiles) to image the whole NSSL in latitude and longitude.

As noted in Section 4.1, the latitudinal extent of negative $\delta(\partial \log \Omega / \partial \log r)$ at $0.95 R_{\odot}$, unlike in the near-surface layers, is narrow and lacks a clear correspondence with δU_{θ} . We point out that understanding these features requires consideration of additional physics involving the radial component of circulating flows (P. A. Gilman 1992; H. C. Spruit 2003) acted on by the nontraditional second term in the full expression for the azimuthal (W–E) component of the Coriolis force: $-2(\mathbf{\Omega} \times \delta \mathbf{U})_{\phi} = 2\Omega \sin(\theta) \delta U_{\theta} - 2\Omega \cos(\theta) \delta U_r$. Here, an upflow ($\delta U_r > 0$) deflects eastward (on the Sun) opposing the rotation while a downflow deflects westward enhancing it; since these effects go as $\cos(\theta)$, they are at their maximum at the equator. Near $0.95 R_{\odot}$, the radial flow amplitudes are in the range of $0.5\text{--}1 \text{ m s}^{-1}$ (S. P. Rajaguru & H. M. Antia 2015; L. Gizon et al. 2020),¹⁰ which will experience comparable azimuthal Coriolis acceleration as that by a meridional flow of 5 m s^{-1} near 10° latitude. Hence, we believe that while the near-surface

¹⁰ Mass conservation constraints in meridional flow inversions yield $U_r(\theta, r)$ profiles too.

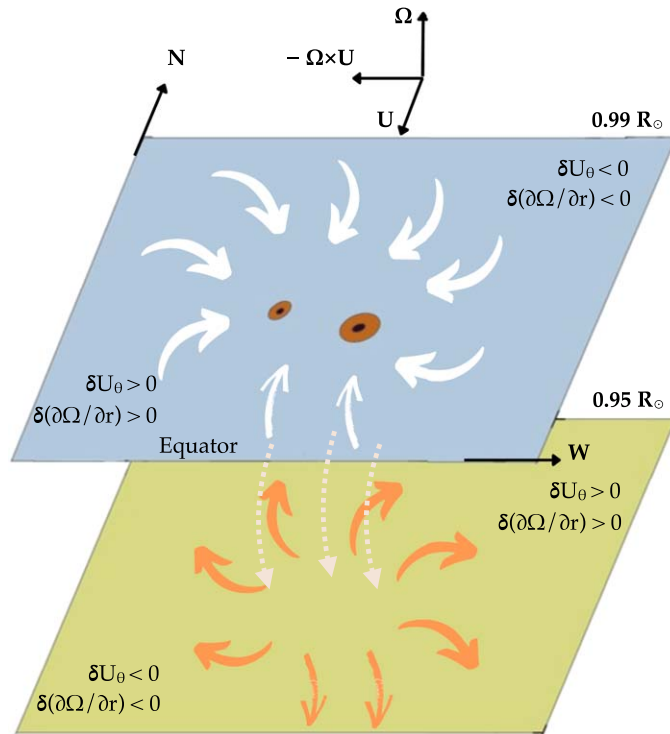


Figure 5. Sketch showing the Coriolis force mediated average flow structures around active regions in the northern hemisphere. The labels depict the signs of residuals in meridional flows, δU_θ , and that of resulting residual rotational shear for the two depths, $0.99 R_\odot$ and $0.95 R_\odot$, which mark the radial boundaries of the NSSL. Figure artwork credit: Amrita Rajaguru.

dynamics is dominated by the Coriolis force on the horizontal component of meridional flows, the deeper layers' dynamics at low latitudes could be influenced significantly by the Coriolis force on the radial flows.

As to the origin of inflows toward active regions, H. C. Spruit (2003) proposed the subsurface temperature variations caused by the increased radiative losses through the plages and small-scale magnetic fields surrounding sunspots. However, our results in Figures 2 and 3 show that, near the active latitudes (20° and 25°) and during the solar maximum, the outflows below $0.97 R_\odot$ have a larger hemispheric asymmetry in proportion to that in the magnetic field than the inflows do near the surface. This runs counter to the expected stronger correlation of near-surface cooling driven inflows with magnetic flux. Thus, our results raise the interesting possibility of large-scale active region flows being driven at a deeper location within the NSSL, similar to an earlier reported finding based on travel-time signatures alone (J. G. Beck et al. 2002). Here, we would like to draw attention to the proposal by P. A. Gilman (1992), based on the dynamics of “thermal shadows” discussed by E. N. Parker (1987), wherein a broad bundle of toroidal field near the base of the convection zone drives a pair of meridional circulation cells, which share a downflow over the central latitude of the toroidal band. We note that an outflow associated with accumulating active region magnetic field near the base of the NSSL, either due to thermal causes or directly due to emergence and horizontal separation, could draw fluid from the overlying layers initiating downflows, which then drive inflows near the surface forming a circulation cell, similar to the proposal of P. A. Gilman (1992) for the fields near the tachocline. We anticipate closer and more detailed examinations of our findings in the near future, as such studies are crucial to

understanding the origin of zonal and meridional flows and their fundamental connections to solar magnetism.

Irrespective of the basic causes behind them, our findings, especially those in Figure 3, show that the meridional and zonal flows have correlated variations over solar cycle timescales, although the amplitudes of the latter change only marginally (see Figure 2). We conclude that the Coriolis force on the residual meridional flows causes the change in the radial gradient of zonal flows within the NSSL, while the driving of the zonal flow itself is likely of deeper origin. We point out, in closing, that the close agreements and correlated variations between the depth profiles of changes in rotation gradient and in meridional flows measured in this work from the quite different global and local helioseismic techniques, respectively, provide an important validation for the measurement procedures, especially for the latter.

Acknowledgments

The HMI data used are courtesy of NASA/SDO and the HMI science teams. Data preparation and processing have utilized the Data Record Management System (DRMS) software at the Joint Science Operations Center (JSOC) for NASA/SDO at Stanford University. We acknowledge that the global helioseismic inversions of solar interior rotation used in this work are from the published results of H. M. Antia, who we thank for sharing them. We also thank the two anonymous reviewers, whose extensive critical reviews and suggestions contributed substantially to the interpretation and presentation of results in this Letter. We accord special credit to one of the reviewers for suggestions on Figure 5. The GONG data used are obtained by the NSO Integrated Synoptic Program, managed by the National Solar Observatory, which is operated by the Association of Universities for Research in Astronomy (AURA), Inc., under a cooperative agreement with the National

Science Foundation and with contribution from the National Oceanic and Atmospheric Administration. This work has received funding from the NASA DRIVE Science Center COFFIES Phase II CAN 80NSSC22M0162 to Stanford University. S.K. was partly supported by NASA grants 80NSSC21K0735, 80NSSC19K0261, and 80NSSC20K0194 to NSO. Data-intensive computations in this work have utilized the High-Performance Computing facility at the Indian Institute of Astrophysics. A.S. is supported by the INSPIRE Fellowship from the Department of Science and Technology (DST), Government of India. S.P.R. acknowledges support from the Science and Engineering Research Board (SERB, Government of India) grant CRG/2019/003786.

ORCID iDs

Anisha Sen  <https://orcid.org/0000-0003-2694-3288>
 S. P. Rajaguru  <https://orcid.org/0000-0003-0003-4561>
 Abhinav Govindan Iyer  <https://orcid.org/0000-0001-8042-2358>
 Ruizhu Chen  <https://orcid.org/0000-0002-2632-130X>
 Junwei Zhao  <https://orcid.org/0000-0002-6308-872X>

References

- Antia, H. M., & Basu, S. 2001, *ApJL*, 559, L67
 Antia, H. M., & Basu, S. 2010, *ApJ*, 720, 494
 Antia, H. M., & Basu, S. 2022, *ApJ*, 924, 19
 Antia, H. M., Basu, S., & Chitre, S. M. 1998, *MNRAS*, 298, 543
 Barekat, A., Schou, J., & Gizon, L. 2014, *A&A*, 570, L12
 Barekat, A., Schou, J., & Gizon, L. 2016, *A&A*, 595, A8
 Beck, J. G., Gizon, L., & Duvall, T. L. 2002, *ApJL*, 575, L47
 Brandenburg, A. 2005, *ApJ*, 625, 539
 Braun, D. C. 2019, *ApJ*, 873, 94
 Braun, D. C. 2024, *ApJ*, 972, 160
 Cameron, R. H., & Schüssler, M. 2010, *ApJ*, 720, 1030
 Cameron, R. H., & Schüssler, M. 2012, *A&A*, 548, A57
 Chen, R., & Zhao, J. 2017, *ApJ*, 849, 144
 Corbard, T., & Thompson, M. J. 2002, *SoPh*, 205, 211
 Dikpati, M., Corbard, T., Thompson, M. J., & Gilman, P. A. 2002, *ApJL*, 575, L41
 Duvall, T. L., Jefferies, S. M., Harvey, J. W., & Pomerantz, M. A. 1993, *Natur*, 362, 430
 Gilman, P. A. 1992, in ASP Conf. Ser. 27, The Solar Cycle, ed. K. L. Harvey (San Francisco, CA: ASP), 241
 Gizon, L., Cameron, R. H., Pourabedian, M., et al. 2020, *Sci*, 368, 1469
 Gizon, L., Duvall, T. L., J., & Larsen, R. M. 2001, in IAU Symp. 203, Recent Insights into the Physics of the Sun and Heliosphere: Highlights from SOHO and Other Space Missions, ed. P. Brekke, B. Fleck, & J. B. Gurman (Cambridge: Cambridge Univ. Press), 189
 González Hernández, I., Kholikov, S., Hill, F., Howe, R., & Komm, R. 2008, *SoPh*, 252, 235
 Gottschling, N., Schunker, H., Birch, A. C., Löptien, B., & Gizon, L. 2021, *A&A*, 652, A148
 Haber, D. A., Hindman, B. W., Toomre, J., & Thompson, M. J. 2004, *SoPh*, 220, 371
 Hindman, B. W., Haber, D. A., & Toomre, J. 2009, *ApJ*, 698, 1749
 Karak, B. B., & Cameron, R. 2016, *ApJ*, 832, 94
 Kitchatinov, L. L. 2016, *AstL*, 42, 339
 Kitchatinov, L. L. 2023, *AstL*, 49, 754
 Komm, R. 2022, *SoPh*, 297, 99
 Lebedinsky, A. 1941, *AZh*, 18, 10
 Liang, Z.-C., & Chou, D.-Y. 2015, *ApJ*, 805, 165
 Mahajan, S. S., Sun, X., & Zhao, J. 2023, *ApJ*, 950, 63
 Matilsky, L. I., Hindman, B. W., & Toomre, J. 2019, *ApJ*, 871, 217
 Miesch, M. S. 2000, *SoPh*, 192, 59
 Parker, E. N. 1987, *ApJ*, 321, 984
 Pipin, V. V., & Kosovichev, A. G. 2011, *ApJL*, 727, L45
 Poulter, P. L., Liang, Z. C., Fournier, D., & Gizon, L. 2022, *A&A*, 664, A189
 Rajaguru, S. P., & Antia, H. M. 2015, *ApJ*, 813, 114
 Scherrer, P. H., Schou, J., & Bush, R. I. 2012, *SoPh*, 275, 207
 Schou, J., Antia, H. M., Basu, S., et al. 1998, *ApJ*, 505, 390
 Spruit, H. C. 2003, *SoPh*, 213, 1
 Teweldeberhan, K., Miesch, M., & Gibson, S. 2024, *SoPh*, 299, 42
 Thompson, M. J., Toomre, J., Anderson, E. R., et al. 1996, *Sci*, 272, 1300
 Vorontsov, S. V., Christensen-Dalsgaard, J., Schou, J., Strakhov, V. N., & Thompson, M. J. 2002, *Sci*, 296, 101
 Zhao, J., Bogart, R. S., Kosovichev, A. G., Duvall, T. L., & Hartlep, T. 2013, *ApJL*, 774, L29
 Zhao, J., Couvidat, S., Bogart, R. S., et al. 2012a, *SoPh*, 275, 375
 Zhao, J., Nagashima, K., Bogart, R. S., Kosovichev, A. G., & Duvall, T. L. 2012b, *ApJL*, 749, L5